

Article

Chiral Conducting Me-EDT-TTF and Et-EDT-TTF-Based Radical Cation Salts with the Perchlorate Anion

Nabil Mroweh ¹, Pascale Auban-Senzier ², Nicolas Vanthuyne ³ , Elsa B. Lopes ⁴,
Manuel Almeida ⁴ , Enric Canadell ⁵  and Narcis Avarvari ^{1,*} 

¹ MOLTECH-Anjou, UMR 6200, CNRS, UNIV Angers, 2 bd Lavoisier, CEDEX, 49045 Angers, France; nabil.mroweh@cea.fr

² Laboratoire de Physique des Solides, Université Paris-Saclay CNRS UMR 8502, Bât. 510, 91405 Orsay, France; pascale.senzier@universite-paris-saclay.fr

³ CNRS, Centrale Marseille, iSm2, Aix Marseille Université, 13397 Marseille, France; nicolas.vanthuyne@univ-amu.fr

⁴ Centro de Ciências e Tecnologias Nucleares (C²TN) and Departamento de Engenharia e Ciências Nucleares (DECN), Instituto Superior Técnico (IST), Universidade de Lisboa, E.N. 10, 2695-066 Bobadela LRS, Portugal; eblopes@ctn.tecnico.ulisboa.pt (E.B.L.); malmeida@ctn.tecnico.ulisboa.pt (M.A.)

⁵ Campus de la UAB, Institut de Ciència de Materials de Barcelona, ICMA-B-CSIC, 08193 Bellaterra, Spain; canadell@icmab.es

* Correspondence: narcis.avarvari@univ-angers.fr; Tel.: +33-(24)-173-5084

Received: 10 November 2020; Accepted: 19 November 2020; Published: 23 November 2020



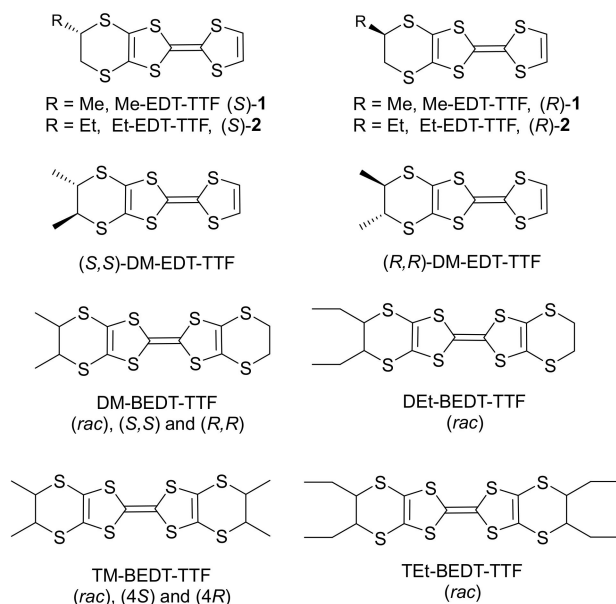
Abstract: Introduction of chirality in the field of molecular conductors has received increasing interest in recent years in the frame of modulation of the crystal packing, and hence conducting properties, with the number of stereogenic centers and absolute configuration, e.g., racemic or enantiopure forms. Here, we describe the preparation by electrocrystallization of chiral radical cation salts, based on the donors methyl-ethylenedithio-tetrathiafulvalene (Me-EDT-TTF) **1** and ethyl-ethylenedithio-tetrathiafulvalene (Et-EDT-TTF) **2** containing one stereogenic center, with the perchlorate anion. Donor **1** provided the series of crystalline materials [(*rac*)-**1**]ClO₄, [(*S*)-**1**]₂ClO₄ and [(*R*)-**1**]₂ClO₄, while for donor **2** only the 1:1 salts [(*rac*)-**2**]ClO₄ and [(*R*)-**2**]ClO₄ could be prepared as suitable single crystals for X-ray analysis. The enantiopure salts of **1** show β -type packing and metallic conductivity in the high temperature regime, with room temperature conductivity values of 5–10 S cm⁻¹, whereas compound [(*rac*)-**2**]ClO₄ is a very poor semiconductor. Tight-binding extended Hückel band structure calculations support the metallic conductivity of the enantiopure salts of **1** and suggest that small structural changes, possibly induced by thermal contraction or pressure, could lead to a pseudo-elliptic closed Fermi surface, typical for a 2D metal.

Keywords: organic conductors; chirality; tetrathiafulvalene; crystal structures; electrical resistivity; band structure calculations

1. Introduction

In the frame of the increasingly developing field of chiral molecular materials [1], we recently introduced methyl-ethylenedithio-tetrathiafulvalene (Me-EDT-TTF) **1** and ethyl-ethylenedithio-tetrathiafulvalene (Et-EDT-TTF) **2** (Scheme 1) as valuable precursors for chiral molecular conductors [2,3], through a series of radical cation salts with the PF₆⁻ anion, in which modulation of the donor:anion stoichiometry, crystal packing and conducting properties with the absolute configuration and steric bulkiness of the substituent was observed [4]. Interesting differences were observed,

for example, between the enantiopure PF_6^- salts of **1** and those of the dimethylated donor DM-EDT-TTF (Scheme 1), since the former crystallize in the triclinic space group $P1$ and show metallic behaviour in the high-temperature regime, while the latter crystallize in the monoclinic space group $P2_1$ and are bandgap semiconductors [5]. These results point out the importance of the number of stereogenic centres in the modulation of intermolecular interactions with the anion, through the establishment of C–H...F hydrogen bonding, donor packing, and thus electron transport properties. Moreover, the (*rac*), (*S*) and (*R*) (**1**) $_2\text{PF}_6$ salts are isostructural with the (DM-EDT-TTF) $_2\text{XF}_6$ ($X = \text{As}, \text{Sb}$) series [6], showing that the size of the anion, in conjunction with the number of stereogenic centres, can also play a paramount role in the modulation of the intermolecular interactions. Enantiopure monoalkylated EDT-TTF **1** and **2** and derivatives [7] have afforded so far only the PF_6^- series of radical cation salts. Comparatively, since the first report of an enantiopure TTF precursor, namely (*S,S,S,S*)-TM-BEDT-TTF [8], enantiopure dimethylated EDT-TTF (DM-EDT-TTF) [5,6,9] and BEDT-TTF (DM-BEDT-TTF) [10–12], together with the tetramethylated BEDT-TTF (TM-BEDT-TTF) [13–16] (Scheme 1), provided several series of radical cation salts, culminating in the first observation of the electrical magnetochiral anisotropy effect (eMChA) in a bulk crystalline conductor [17]. Note that diethyl BEDT-TTF (DEt-BEDT-TTF) and tetraethyl BEDT-TTF (TEt-BEDT-TTF) (Scheme 1) precursors have been reported only in the racemic form [18]. Besides the hexafluorophosphate, another anion very often encountered in TTF based radical cation salts, including in the chiral ones, is the perchlorate. Indeed, enantiopure DM-EDT-TTF provided enantiomorphic mixed-valence salts (DM-EDT-TTF) $_2\text{ClO}_4$ showing the eMChA effect [17], the use of (*S,S,S,S*)-TM-BEDT-TTF afforded a 3:2 salt with metallic conductivity [13], while an orthorhombic semiconducting phase [11] and a metallic monoclinic phase [19], both presenting a 2:1 stoichiometry, have been reported for (*R,R*)-DM-BEDT-TTF and (*S,S*)-DM-BEDT-TTF, respectively. Moreover, a superconducting transition was suggested for the latter [19], yet this assumption was recently invalidated by more complete physical measurements on both enantiomeric salts [20].



Scheme 1. Methyl and ethyl substituted ethylenedithio-tetrathiafulvalene (EDT-TTF) and bis(ethylenedithio)-tetrathiafulvalene (BEDT-TTF) donors.

In the continuation of our research line dedicated to chiral molecular conductors, we describe herein the synthesis, structural characterization and electron transport properties of racemic and enantiopure radical cation salts of Me-EDT-TTF **1** and Et-EDT-TTF **2** with the perchlorate anion, together with band structure calculations, highlighting some peculiar features of their electronic structures.

2. Materials and Methods

Donors **1** and **2** were prepared as recently described [4]. For each of the three electrocrystallization experiments with **1**, [NBu₄]ClO₄ (20 mg) was dissolved in 6 mL THF and the solution was poured into the cathodic compartment of an electrocrystallization cell. The anodic chamber was filled respectively with 5 mg of (*rac*)-**1**, (*S*)-**1** and (*R*)-**1** dissolved in 6 mL THF. Crystals of each salt grown at 3 °C over a period of one week on a platinum wire electrode, by applying a constant current of 1 μA. Black plates were obtained on the electrode for [(*rac*)-**1**]ClO₄ and brown thin narrow plates for [(*S*)-**1**]₂ClO₄ and [(*R*)-**1**]₂ClO₄. Similar experimental conditions were applied for the electrocrystallization of (*rac*)-**2**, (*S*)-**2** and (*R*)-**2** in the presence of [NBu₄]ClO₄. Black crystalline needles were obtained on the electrode for [(*rac*)-**2**]ClO₄, while for (*R*)-**2** a mixture of small green thin plates, formulated as [(*R*)-**2**]₂ClO₄, and dark violet thick plates, corresponding to [(*R*)-**2**]ClO₄, were collected after several trials. The quality of the former was not sufficient to allow a high quality crystal structure, yet it allowed to clearly identify the components and to determine the packing of the donors. Unfortunately, no salt with (*S*)-**2** crystallized under these conditions.

Single crystals of the compounds were mounted on glass fibre loops using a viscous hydrocarbon oil to coat the crystal and then transferred directly to cold nitrogen stream for data collection. Data collection was performed on an Agilent Supernova diffractometer with CuKα (λ = 1.54184 Å). The structures were solved by direct methods with the SIR92 program and refined against all F² values with the SHELXL-97 program using the WinGX graphical user interface. All non-H atoms were refined anisotropically. Hydrogen atoms were introduced at calculated positions (riding model), included in structure factor calculations but not refined. Further details about data collection and solution refinement are given in Table 1; Table 2.

Crystallographic data for the five structures were deposited with the Cambridge Crystallographic Data Centre, deposition numbers CCDC 2043591 ([(*rac*)-**1**]ClO₄), 2043592 ([(*R*)-**1**]₂ClO₄), 2043593 ([(*S*)-**1**]₂ClO₄), 2043594 ([(*rac*)-**2**]ClO₄), 2043595 ([(*R*)-**2**]ClO₄). These data can be obtained free of charge from CCDC, 12 Union road, Cambridge CB2 1EZ, UK (e-mail: deposit@ccdc.cam.ac.uk or <http://www.ccdc.cam.ac.uk>).

Table 1. Crystal Data for compounds [(*rac*)-**1**]ClO₄, [(*R*)-**1**]₂ClO₄ and [(*S*)-**1**]₂ClO₄.

Compound	[(<i>rac</i>)- 1]ClO ₄	[(<i>R</i>)- 1] ₂ ClO ₄	[(<i>S</i>)- 1] ₂ ClO ₄
formula	C ₉ H ₈ ClO ₄ S ₆	C ₁₈ H ₁₆ ClO ₄ S ₁₂	C ₁₈ H ₁₆ ClO ₄ S ₁₂
M (g mol ⁻¹)	407.96	716.48	716.48
(T)	150.00(10)	155.00(7)	170.58(10)
crystal system	Triclinic	Monoclinic	Monoclinic
space group	<i>P</i> -1	<i>C</i> 2	<i>C</i> 2
<i>a</i> (Å)	6.4126(4)	15.1135(5)	15.1561 (5)
<i>b</i> (Å)	9.4439(6)	6.5681(2)	6.5791(2)
<i>c</i> (Å)	12.2713(8)	26.6686(9)	26.6154(9)
α (°)	97.293(5)	90	90
β (°)	94.927(5)	091.898(3)	91.828(3)
γ (°)	96.828(5)	90	90
<i>V</i> (Å ³)	728.05(8)	2645.86(15)	2652.56(15)
<i>Z</i>	2	4	4
ρ _{calcd} (g cm ⁻³)	1.861	1.799	1.794
μ (mm ⁻¹)	10.464	10.390	10.364
Flack parameter	-	0.06(2)	0.04(4)
Completeness (%)	99.1%	99.5%	99.8%
goodness-of-fit on F ²	1.061	1.081	1.040
final R1/wR2 [I > 2σ(I)]	R1 = 0.0676, wR2 = 0.1781	R1 = 0.0611, wR2 = 0.1583	R1 = 0.0515, wR2 = 0.1331
R1/wR2 (all data)	R1 = 0.0809, wR2 = 0.1903	R1 = 0.0629, wR2 = 0.1597	R1 = 0.0560, wR2 = 0.1361

Table 2. Crystal Data for compounds [(*rac*)-2]ClO₄ and [(*R*)-2]ClO₄.

Compound	[(<i>rac</i>)-2]ClO ₄	[(<i>R</i>)-2]ClO ₄
formula	C ₁₀ H ₁₀ ClO ₄ S ₆	C ₁₀ H ₁₀ ClO ₄ S ₆
<i>M</i> (g mol ⁻¹)	421.99	421.99
<i>T</i> (K)	150.00(10)	150.00(10)
crystal system	Triclinic	Triclinic
space group	<i>P</i> -1	<i>P</i> 1
<i>a</i> (Å)	7.5501(9)	7.5729(5)
<i>b</i> (Å)	9.3157(10)	9.1781(6)
<i>c</i> (Å)	11.7417(11)	11.8048(9)
α (°)	80.593(9)	80.392(6)
β (°)	75.196(11)	76.155(6)
γ (°)	79.910(9)	81.022(6)
<i>V</i> (Å ³)	779.95(14)	779.68(9)
<i>Z</i>	2	2
ρ_{calcd} (g cm ⁻³)	1.797	1.797
μ (mm ⁻¹)	9.791	9.794
Flack parameter	-	0.10(6)
Completeness (%)	99.5%	97.1%
goodness-of-fit on <i>F</i> ²	1.047	1.049
final <i>R</i> 1/ <i>wR</i> 2 [<i>I</i> > 2 σ (<i>I</i>)]	<i>R</i> 1 = 0.0662, <i>wR</i> 2 = 0.1751	<i>R</i> 1 = 0.0531, <i>wR</i> 2 = 0.1423
<i>R</i> 1/ <i>wR</i> 2 (all data)	<i>R</i> 1 = 0.0795, <i>wR</i> 2 = 0.1981	<i>R</i> 1 = 0.0574, <i>wR</i> 2 = 0.1487

Electrical conductivity and the thermoelectric power measurements for [(*S*)-1]₂ClO₄ and [(*R*)-1]₂ClO₄ single crystals were made along the long axis of the crystals (*a* axis) in the temperature range of 20/50–310 K, using a measurement cell attached to the cold stage of a closed-cycle helium refrigerator. The thermopower was measured by using a slow AC (ca. 10² Hz) technique [21], by attaching two $\varnothing = 25$ μm diameter 99.99% pure Au wires (Goodfellow, UK), thermally anchored to two quartz blocks, with Pt paint (Demetron, Germany, 308A) to the extremities of an elongated sample as in a previously described apparatus [22], controlled by a computer [23]. The oscillating thermal gradient was kept below 1 K and was measured with a differential Au 0.05 at. % Fe vs. chromel thermocouple of the same type. The absolute thermoelectric power of the samples was obtained after correction for the absolute thermopower of the Au leads, by using the data of Huebner [24]. Electrical resistivity measurements were done both in a four-in-line contact configuration, using a low-frequency AC method (77 Hz) with a 5–10 μA current, the voltage is measured with an SRS (Stanford Research Systems, California, USA) Model SR83 lock-in amplifier, and in two points configuration. For resistivity measurements with two contacts, gold wires were glued with silver paste directly on both ends of the crystals and low temperature was provided by a homemade cryostat equipped with a 4 K pulse-tube. For [(*S*)-1]₂ClO₄ and [(*R*)-1]₂ClO₄ single crystals, we applied a DC current (0.1 μA) and measured the voltage with a Keithley 2401 microvoltmeter (Tektronix, Inc Beaverton, OR 97077 United States). Note that, in this configuration, the resistance of the two contacts is added to the resistance of the sample which makes it difficult to evidence a metallic behavior when cooling down. For measuring much higher resistance values in [(*rac*)-2]ClO₄ and [(*R*)-2]ClO₄ single crystals, we used a different technique always in two points configuration. We applied a constant voltage (10–15 V) and measured the current using a Keithley 6487 Picoammeter/Voltage Source (Tektronix, Inc Beaverton, OR 97077 United States). However, [(*R*)-2]ClO₄ single crystals could not be cooled down because the limit in current detection (around 50 pA) was nearly reached at room temperature.

The tight-binding band structure calculations were of the extended Hückel type [25]. A modified Wolfsberg–Helmholtz formula was used to calculate the non-diagonal $H_{\mu\nu}$ values [26]. All valence electrons were taken into account in the calculations and the basis set consisted of Slater-type orbitals of

double- ζ quality for C 2s and 2p, S 3s and 3p and of single- ζ quality for H 1s. The ionization potentials, contraction coefficients and exponents were taken from previous work [27].

3. Results and Discussion

Donors **1** and **2** were prepared as racemic mixtures according to the protocol we recently reported, followed by chiral HPLC separation to afford the pure enantiomers [4]. The racemic and enantiopure forms of both donors were engaged in electrocrystallization experiments in the presence of $[\text{NBu}_4]\text{ClO}_4$ as a supporting electrolyte. Suitable single crystals for X-ray diffraction analysis of radical cation salts with ClO_4^- were obtained for (*rac*)-**1**, (*R*)-**1**, (*S*)-**1**, (*rac*)-**2** and (*R*)-**2**.

3.1. Solid-State Structures of the Radical Cation Salts

3.1.1. $[(rac)\text{-1}]\text{ClO}_4$, $[(R)\text{-1}]_2\text{ClO}_4$ and $[(S)\text{-1}]_2\text{ClO}_4$

Black thick crystalline plates of $[(rac)\text{-1}]\text{ClO}_4$ were collected on the electrode. The compound crystallizes in the triclinic centrosymmetric space group $P\bar{1}$, with one independent donor molecule and one anion in the asymmetric unit (Figure 1a). The methyl substituent lies in the axial position and the oxygen atom O1 is disordered over two positions O1A (s.o.f. 0.28) and O1B (s.o.f. 0.72).

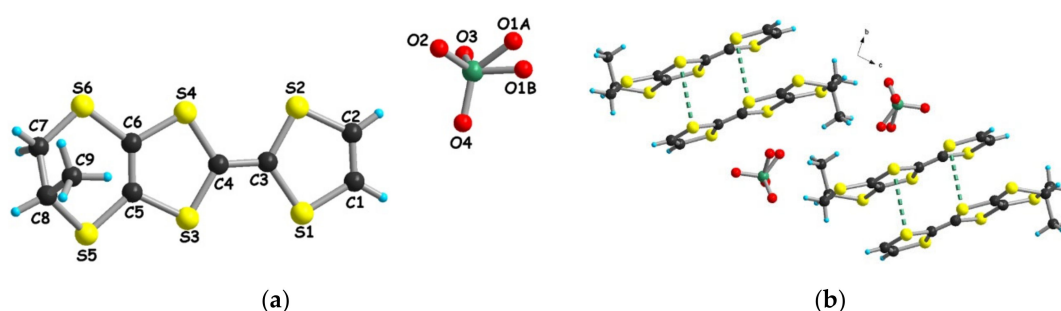


Figure 1. (a) Molecular structure of $[(rac)\text{-1}]\text{ClO}_4$ (O1 atom is disordered). Only the (*S*) enantiomer of the donor is shown; (b) Packing diagram of $[(rac)\text{-1}]\text{ClO}_4$ in the *bc* plane, with an emphasis on the intradimer $\text{S}\cdots\text{S}$ short contacts (3.38 and 3.47 Å, green dotted lines).

The donors form very stable centrosymmetric head-to-tail dimers (*vide infra*) through the establishment of very short $\text{S}\cdots\text{S}$ intermolecular contacts of 3.385 and 3.466 Å (Figure 1b). These dimers interact especially laterally along the *a*-direction as denoted by the short $\text{S}\cdots\text{S}$ intermolecular contacts ranging between 3.39 and 3.87 Å (Figure S1). The stoichiometry 1:1 is in favor of a +1 oxidation state of the donors, in agreement with the values of the central C=C and internal C–S bonds (Table 3).

Table 3. Selected C=C and C–S bond lengths for $[(rac)\text{-1}]\text{ClO}_4$, $[(R)\text{-1}]_2\text{ClO}_4$ and $[(S)\text{-1}]_2\text{ClO}_4$.

		Bond Lengths (Å)			
		$[(R)\text{-1}]_2\text{ClO}_4$	$[(S)\text{-1}]_2\text{ClO}_4$	$[(rac)\text{-1}]\text{ClO}_4$	
A	compound			C3—C4	1.390(8)
	C3A—C4A	1.385(13)	1.372(8)	S1—C3	1.721(6)
	S1A—C3A	1.738(10)	1.746(6)	S2—C3	1.715(6)
	S2A—C3A	1.731(10)	1.729(6)	S3—C4	1.710(6)
	S3A—C4A	1.720(9)	1.749(6)	S4—C4	1.722(5)
B	S4A—C4A	1.730(10)	1.730(6)	—	—
	C3B—C4B	1.368(13)	1.392(7)	—	—
	S1B—C3B	1.744(9)	1.734(6)	—	—
	S2B—C3B	1.736(10)	1.733(6)	—	—
	S3B—C4B	1.750(10)	1.711(5)	—	—
S4B—C4B	1.733(10)	1.726(6)	—	—	

As already extensively discussed for the $(1)_2\text{PF}_6$ series of salts [4], the anion is also involved here in several hydrogen-bonding interactions between the oxygen atoms and protons of different types (CH_{vinyl} , CH_{Me} , CH_2 and CH_3) (Figure S2).

The enantiopure salts $[(R)\text{-}1]_2\text{ClO}_4$ and $[(S)\text{-}1]_2\text{ClO}_4$ are isostructural and crystallize in the monoclinic non-centrosymmetric space group $C2$, the asymmetric unit containing two independent donor molecules and two anion halves located on C_2 symmetry axes. Unlike the racemic salt, now the methyl substituent is located in an equatorial position in both independent molecules (Figure 2a for the (R) enantiomer). Since the two compounds are isostructural, only $[(R)\text{-}1]_2\text{ClO}_4$ will be detailed hereafter. Parallel columns of donors oriented in a head-to-tail manner are present in the organic layer, an arrangement reminiscent of the β -type packing [28]. Intrastack and interstack short $\text{S}\cdots\text{S}$ contacts of 3.52–3.54 Å and 3.62–3.63 Å, respectively, are observed (Figure 2b).

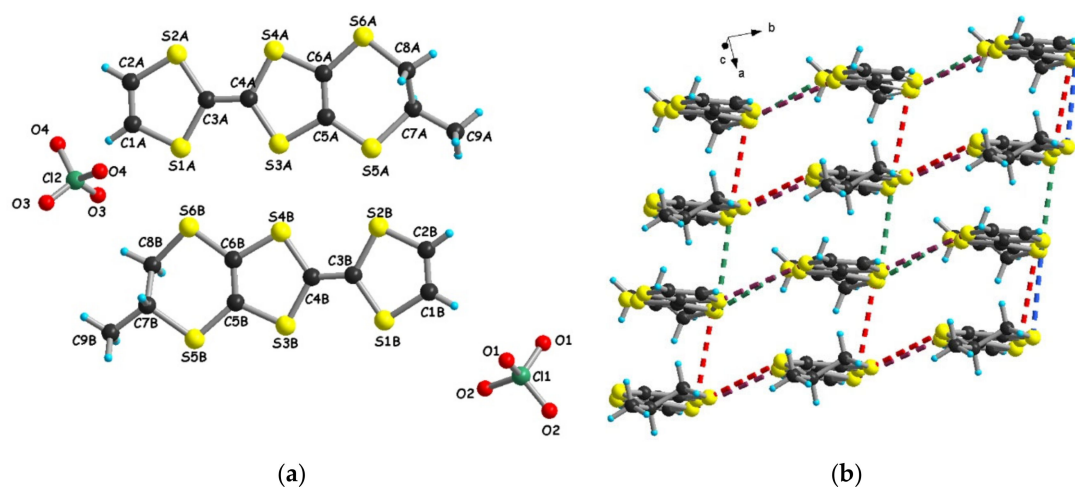


Figure 2. (a) Molecular structure of $[(R)\text{-}1]_2\text{ClO}_4$ along with the atom numbering scheme; (b) Donor layer with an emphasis on the $\text{S}\cdots\text{S}$ short contacts: red dotted lines (3.52–3.54 Å), blue dotted lines (3.81 Å), green dotted lines (3.62–3.63 Å) and violet dotted lines (4.02 Å).

The analysis of the central $\text{C}=\text{C}$ and internal $\text{C}-\text{S}$ bond lengths (Table 3) suggests that the charge is equally distributed over the two independent donor molecules which are thus in a mixed-valence state. Again, the anions and the donors engage in a set of hydrogen bond interactions, such as $\text{CH}_{\text{vinyl}}\cdots\text{O}$ (2.43–2.51 Å), $\text{H}_{\text{CH}_2}\cdots\text{O}$ (2.46–2.63 Å) and $\text{H}_{\text{Me}}\cdots\text{O}$ (2.62 Å) (Figure 3).

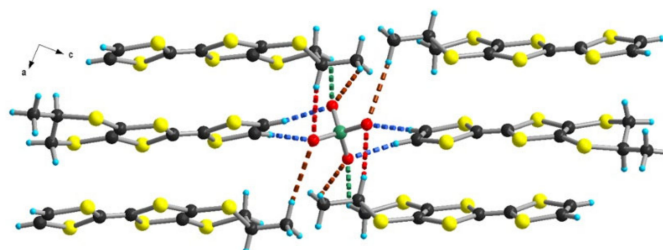


Figure 3. Solid-state structure of $[(R)\text{-}1]_2\text{ClO}_4$, with an emphasis on the $\text{C}-\text{H}\cdots\text{O}$ short contacts: blue dotted lines for CH_{vinyl} (2.43–2.51 Å), green dotted lines for CH_2 (2.46–2.63 Å), brown dotted lines for Me (2.62 Å) and red dotted line for CH_{Me} (2.99 Å).

The crystal structures of $[(R)\text{-}1]_2\text{ClO}_4$ and $[(S)\text{-}1]_2\text{ClO}_4$ are thus completely different from those of the analogous salts with the dimethylated donor DM-EDT-TTF, i.e., $[(R,R)\text{-DM-EDT-TTF}]_2\text{ClO}_4$ and $[(S,S)\text{-DM-EDT-TTF}]_2\text{ClO}_4$, which crystallized in hexagonal enantiomorphous space groups [17], pointing out the importance of the number of stereogenic centers in the modulation of the packing.

3.1.2. [(rac)-2]ClO₄ and [(R)-2]ClO₄

Electrocrystallization of donor **2** provided crystalline materials only for the racemic and (R) enantiomer, with two different phases of 1:1 and 2:1 stoichiometry for the latter. However, the crystals of the [(R)-2]₂ClO₄ phase were not of sufficient quality to allow an accurate description of the structure, yet the packing of the donors is similar to the one in [(R)-1]₂ClO₄ (*vide supra*). [(rac)-2]ClO₄ crystallized in the triclinic system, *P*-1 space group, with one independent donor and one anion in the asymmetric unit (Figure 4a), while [(R)-2]ClO₄, which is isostructural to the racemic counterpart, crystallized in the non-centrosymmetric space group *P*1 of the triclinic system, with two donors and two anions in the asymmetric unit (Figure S3).

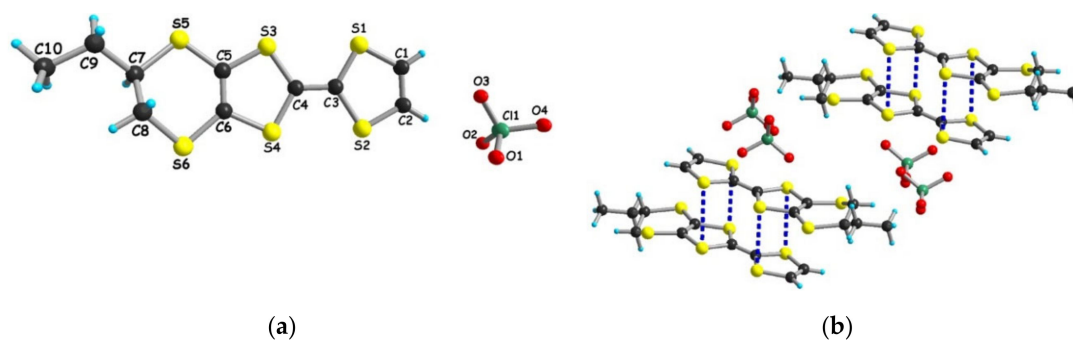


Figure 4. (a) Molecular structure of [(rac)-2]ClO₄ along with the atom numbering scheme. Only the (R) enantiomer of the donor is shown; (b) Packing diagram of [(rac)-2]ClO₄, with an emphasis on the intradimer S...S short contacts (3.37 and 3.47 Å, blue dotted lines).

According to the 1:1 stoichiometry the donors should bear a +1 charge, in agreement with the central C=C and internal C–S bond lengths (Table S1). In both structures the ethyl substituents are located in the equatorial position, although the donors arrange in head-to-tail dimers as in [(rac)-1]ClO₄ where the methyl substituent is axial, with very short intradimer S...S distances of 3.37–3.47 Å for [(rac)-2]ClO₄ (Figure 4b) and 3.35–3.37 Å for [(R)-2]ClO₄ (Figure S4). This strong dimerization should lead, very likely, to rather poor electron transport properties (*vide infra*). As in the case of donor **1**, a complex set of hydrogen bond interactions between the oxygen atoms of the anion and the hydrogen atoms of the donors can be disclosed (Figure S5 for [(rac)-2]ClO₄ and Figure S6 for [(R)-2]ClO₄), emphasizing once again the template role of the anion in the structural disposition of the donors.

3.2. Single Crystal Conductivity Measurements

In the (1)₂ClO₄ series only the crystals of the enantiopure phases, namely [(R)-1]₂ClO₄ and [(S)-1]₂ClO₄, were of suitable dimensions for two- and four-contact single-crystal resistivity measurements, although great care had to be taken because of the fragility of the crystalline plates. The measured room temperature conductivity values range between 5–10 S cm^{−1} depending on the quality of the sample and of the contacts. However, the temperature dependence of the resistivity suggests metal-like conductivity in the high-temperature range (partially masked in the two points measurements), followed upon cooling by a localized regime with a very low activation energy of 29–47 meV (340–540 K) (Figure 5a). The thermoelectric power measurements are also indicative of metallic behavior in the high-temperature regime (Figure 5b) when considering the very small positive values decreasing towards zero upon cooling.

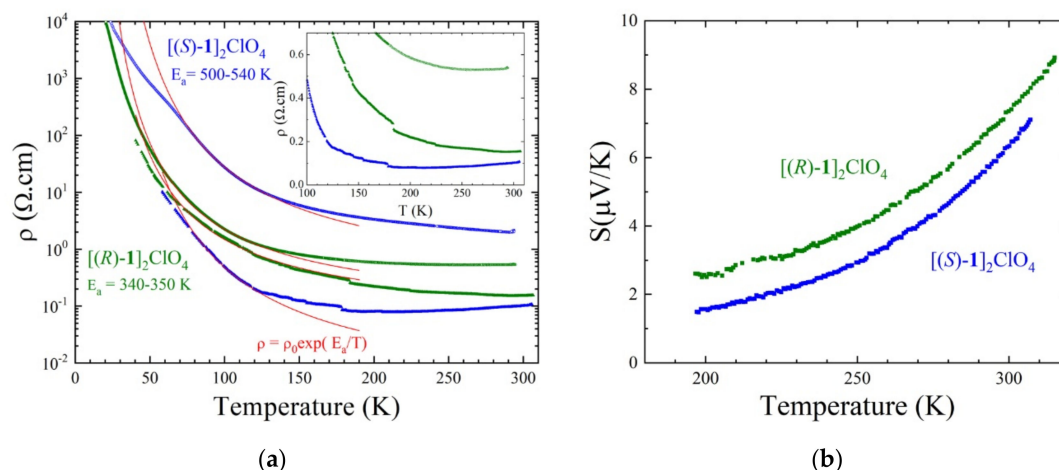


Figure 5. (a) Temperature dependence of the electrical resistivity ρ for single crystals of $[(S)-1]_2\text{ClO}_4$ (blue curves) and $[(R)-1]_2\text{ClO}_4$ (green curves) measured using either four in-line contacts (two lower curves, full symbols) or two contacts (two upper curves, empty symbols). The red lines are the fit to the activation law $\rho = \rho_0 \exp(E_a/T)$ in the 80–130 K temperature range. The inset shows the same resistivity data on a linear scale in order to emphasize the high temperature conducting regime in the three lower curves. (b) Temperature dependence of the thermoelectric power for a single crystal of $[(S)-1]_2\text{ClO}_4$ (blue curve) and $[(R)-1]_2\text{ClO}_4$ (green curve).

The 2:1 stoichiometry and β -type packing of the donors in $[(R)-1]_2\text{ClO}_4$ and $[(S)-1]_2\text{ClO}_4$ are clearly in favor of high electrical conductivity in the organic layer, as suggested by the single crystal electrical resistivity measurements. The situation is drastically different in the case of $(2)\text{ClO}_4$ salts. Suitable crystals for temperature-dependent resistivity measurements could be obtained only for $[(rac)-2]\text{ClO}_4$. As expected when considering the strong dimerization of the donors in the crystal structure, the room temperature value of the resistivity of $10^7 \Omega \text{ cm}$ and activation energy $E_a = 5100$ K clearly indicate a very poor semiconducting, almost insulating, behavior of this material (Figure 6 and Figure S7). Moreover, a value of $\rho = 2 \times 10^8 \Omega \text{ cm}$ room temperature resistivity could be measured on small crystals of $[(R)-2]\text{ClO}_4$, which are isostructural with the racemic form.

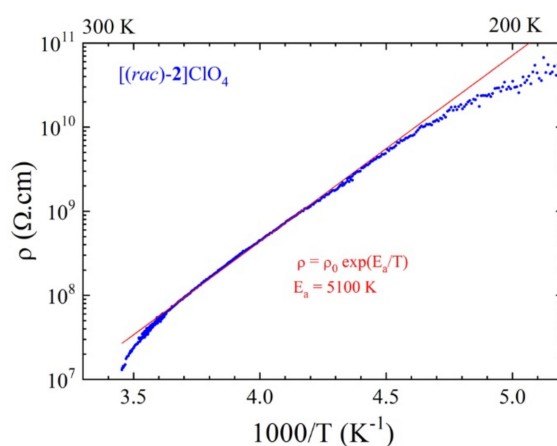


Figure 6. Temperature dependence of the electrical resistivity, ρ , plotted as $\log \rho$ versus $1000/T$ for a single crystal of $[(rac)-2]\text{ClO}_4$ measured using two contacts. The red line is the linear fit to the data giving the activation energy.

Since the two racemic salts $[(rac)\text{-1}]\text{ClO}_4$ and $[(rac)\text{-2}]\text{ClO}_4$ are structurally very similar it can be inferred that the former is also a poor semiconductor.

3.3. Band Structure Calculations

3.3.1. $[(rac)\text{-1}]\text{ClO}_4$ and $[(rac)\text{-2}]\text{ClO}_4$

Although the samples of $[(rac)\text{-1}]\text{ClO}_4$ did not allow single-crystal resistivity measurements, unlike those of $[(rac)\text{-2}]\text{ClO}_4$, we performed band structure calculations on both racemic salts for comparison purpose. The donor lattice of the $[(rac)\text{-1}]\text{ClO}_4$ salt is shown in Figure 7a, highlighting the presence of dimers. Although there are quite short contacts associated with all interactions (Table 4), the very good σ -type overlap associated with the interaction I should make this interaction largely dominant. Because of the head-to-tail overlap mode the S...S contacts along b - and c - are long. However, note that whereas the methyl substituents practically cut any interaction along c , the donors face each other through the non-substituted side of the molecule along b , providing a better situation for possible inter-dimer interaction. The S...S contacts shorter than 3.9 Å as well as the associated $\beta_{\text{HOMO-HOMO}}$ values are reported in Table 4. Interaction I is almost two orders of magnitude larger than the other interactions, so that this salt must be considered as made of chains, along the a -direction, of very stable $(\text{Me-EDT-TTF}_2)^{2+}$ dimers.

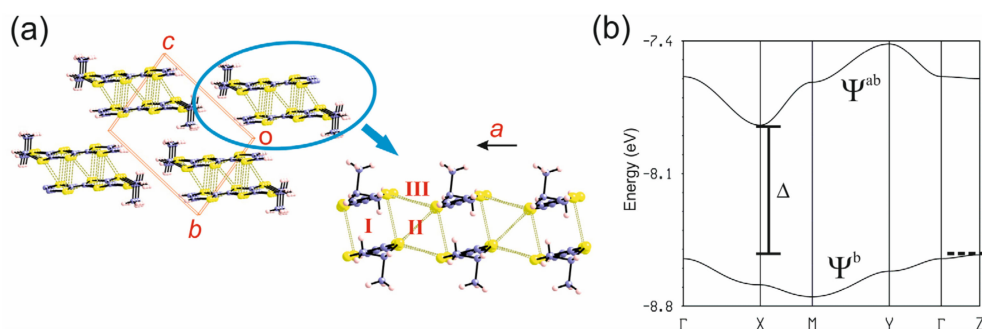


Figure 7. (a) Donor lattice of the $[(rac)\text{-1}]\text{ClO}_4$ salt where the chains and the main intermolecular interactions are labeled; (b) Extended Hückel band structure for the donor lattice of $[(rac)\text{-1}]\text{ClO}_4$. The dashed line refers to the highest occupied level and $\Gamma = (0, 0, 0)$, $X = (a^*/2, 0, 0)$, $Y = (0, b^*/2, 0)$, $M = (a^*/2, b^*/2, 0)$ and $Z = (0, 0, c^*/2)$.

Table 4. Intermolecular S...S contacts shorter than 3.9 Å and absolute values of the $\beta_{\text{HOMO-HOMO}}$ interaction energies (eV) [[29]] for the different donor...donor interactions in the $[(rac)\text{-1}]\text{ClO}_4$ salt.

Interaction	S...S (Å)	$ \beta_{\text{HOMO-HOMO}} $ (eV)
I	3.385 (×2), 3.466 (×2)	0.9401
II	3.518 (×2), 3.793	0.0207
II	3.394, 3.497, 3.839, 3.849, 3.877	0.0401

The calculated band structure is shown in Figure 7b where an indirect bandgap (from Z to X) of 0.67 eV clearly separates the two HOMO bands (i.e., only the lower band, built from the bonding combination of the two HOMOs, Ψ^b , is filled). Note that whereas the dispersion of the lower band is weak, that of the upper one is quite considerable and of the same order along the directions a and b . Thus the effective mass of the electron carriers should be considerably larger than that of the hole carriers and may confer a considerably 2D character to the activated conductivity. The larger dispersion associated with the upper band is a consequence of the antibonding nature of the upper Ψ^{ab} orbital of the dimer for two reasons: (i) because of the inclination of the molecules with respect to the a axis the inter-dimer overlap along this direction is better, and (ii) because of the intra-dimer antibonding character the Ψ^{ab} orbital somewhat hybridizes with molecular σ levels so as to shift the wave function

towards the outer region of the dimer, thus slightly decreasing the antibonding nature of Ψ^{ab} and somewhat favoring the inter-dimer overlap along b .

The calculated band structure for $[(rac)\text{-}2]\text{ClO}_4$ (see Figure S8) leads to an equivalent description and an indirect bandgap of 0.8 eV from Γ to X , in excellent agreement with our conductivity measurements.

3.3.2. $[(R)\text{-}1]_2\text{ClO}_4$ and $[(S)\text{-}1]_2\text{ClO}_4$

The donor layers of the $[(R)\text{-}1]_2\text{ClO}_4$ and $[(S)\text{-}1]_2\text{ClO}_4$ salts contain two different donors and six different intermolecular interactions (see Figure 8). The layer can be described as a series of parallel chains of AB dimers (interaction I) running along the $(a + b)$ -direction. Every donor is implicated in two different interactions along the chain and four inter-chain interactions. To understand the electronic structure and transport properties of these salts we need to have a hint on the strength of the HOMO...HOMO interactions which may be done by looking at the absolute value of the so-called HOMO...HOMO interaction energy, $\beta_{\text{HOMO-HOMO}}$, [29] associated with each interaction. The calculated values for the six interactions in the two different layers of the two pure enantiomeric salts are reported in Table 5.

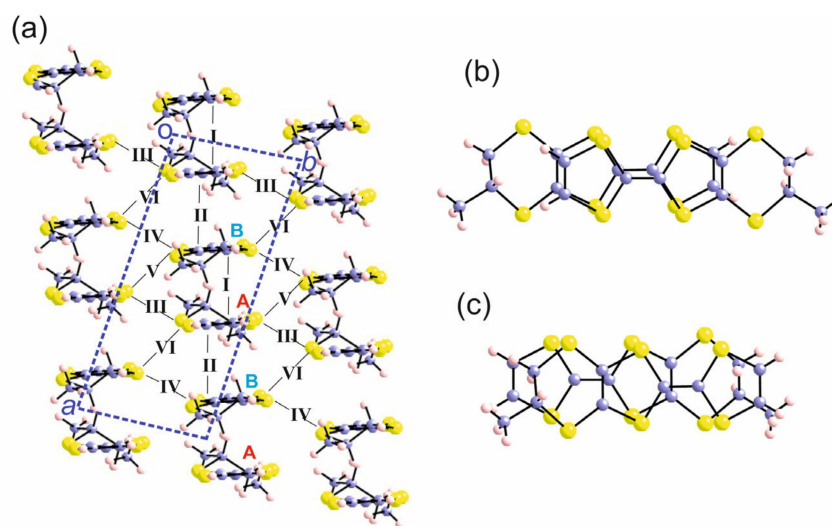


Figure 8. (a) Donor layer of the $[(R)\text{-}1]_2\text{ClO}_4$ salt where the different donors and intermolecular interactions are labeled; (b) Top view of the intra-dimer interaction I; (c) Top view of the inter-dimer interaction II.

Table 5. Absolute values of the $\beta_{\text{HOMO-HOMO}}$ interaction energies (eV) for the different donor...donor interactions in the $[(R)\text{-}1]_2\text{ClO}_4$ and $[(S)\text{-}1]_2\text{ClO}_4$ salts.

Interaction	$[(R)\text{-}1]_2\text{ClO}_4$	$[(S)\text{-}1]_2\text{ClO}_4$
I (A-B)	0.7880	0.7865
II (A-B)	0.6366	0.6285
III (A-A)	0.0303	0.0290
IV (B-B)	0.0370	0.0375
V (A-B)	0.0774	0.0765
VI (A-B)	0.1012	0.0945

The results for both enantiomers are practically identical. The more salient observation is that the interactions along the chain (I and II) are strong whereas the inter-chain interactions (III to VI) are practically one order of magnitude weaker. This should confer a clear one-dimensional (1D) character to the system. Note that the two intra-chain interactions, despite originating from different overlap modes (Figure 8b,c), are associated with similar interaction energy values, showing that a better orientation of the HOMOs (electronic effect) may perfectly compensate for a larger set of short contacts

(metric effect). Because of this fact, the chains along the diagonal ($a + b$)-direction are quite uniform as far as the HOMO...HOMO interactions are concerned. Note that the lateral interactions although weaker are by no means negligible so that they should provide a substantial coupling between these quite uniform chains.

The calculated band structure and Fermi surface of the $[(R)\text{-}1]_2\text{ClO}_4$ salt are shown in Figure 9 (those for $[(S)\text{-}1]_2\text{ClO}_4$ are practically identical as shown in Figure S9). The diagram in Figure 9a contains four HOMO bands because there are four donors per repeat unit. Because of the stoichiometry, there are two holes in these bands so that two partially filled and very dispersive bands are generated, in agreement with the metallic character of these salts. The calculated Fermi surface may appear complex at a first sight although really it is not. The repeat unit of the layer contains two identical AB pairs so that the calculation could have been performed using a centered rectangular lattice with just two molecules in the unit cell. In that case, the calculated Fermi surface would simply be the red part of Figure 9b (and the area of the Brillouin zone would be twice larger). Using the crystallographic repeat unit, which is twice larger, two identical Fermi surfaces are folded into the new, smaller Brillouin zone shown in Figure 9b. The warped red lines of Figure 9b are perpendicular to the ($a + b$)-direction as it must be if the system is built from chains of HOMOs along the ($a + b$)-direction. The warping of the red lines is substantial because of the above noted lateral interactions; in fact the two lines almost touch at the S point so that it is possible that small structural changes brought about by thermal contraction or pressure could maybe close the lines and lead to a pseudo-elliptic closed Fermi surface (i.e., a 2D metal). Note that the red Fermi surface is almost identical to those reported for the $(\text{DM-EDT-TTF})\text{XF}_6$ ($X = \text{P, As, Sb}$) salts [5,6], where the donor possesses two stereogenic centers, as well as for $(1)_2\text{PF}_6$ [4], in which, as in the present salts, the donor has a single stereogenic center, thus denoting a very similar organization of the layers in all these salts. We direct the reader to these references for further discussion of the electronic structure of these layers. However, we note that even if some parts of the red Fermi surface of Figure 9b are nested, such nesting is incomplete. Consequently, if metal to insulator low-temperature transitions occur in these salts, as for some of the above-mentioned ones, it is not expected that they may originate from the charge or spin density wave instabilities so frequent in low dimensional systems but from electronic or structural localization.

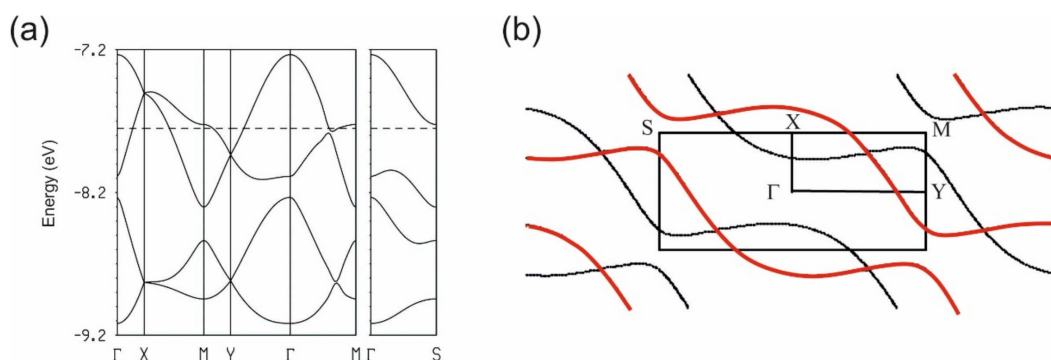


Figure 9. (a) Extended Hückel band structure and (b) Fermi surface for the donor layers of $[(R)\text{-}1]_2\text{ClO}_4$. The dashed line refers to the calculated Fermi level and $\Gamma = (0, 0)$, $X = (a^*/2, 0)$, $Y = (0, b^*/2)$, $M = (a^*/2, b^*/2)$ and $S = (a^*/2, -b^*/2)$.

4. Conclusions

Electrocrystallization of the chiral EDT-TTF derivatives **1** and **2** provided a complete series of radical cation salts for the former and racemic and enantiopure (R) salts for the latter, with the same perchlorate anion. Interestingly, unlike the series with the PF_6^- anion previously described [4], where the racemic and enantiopure salts were isostructural, here, the perchlorate ion discriminates between the racemic and enantiopure forms (Table 6).

Table 6. Comparison between the radical cation salts of donors 1 and 2 with the ClO₄[−] and PF₆[−] anions.

Radical Cation Salt	Stoichiometry (Donor:Anion)	Crystal System	Conductivity (High Temperature)
[(<i>rac</i>)-1]ClO ₄	1:1	Triclinic	Poor semiconductor
[(<i>R</i>)-1] ₂ ClO ₄	2:1	Monoclinic	Metal
[(<i>S</i>)-1] ₂ ClO ₄	2:1	Monoclinic	Metal
[(<i>rac</i>)-1] ₂ PF ₆	2:1	Triclinic	Metal
[(<i>R</i>)-1] ₂ PF ₆	2:1	Triclinic	Metal
[(<i>S</i>)-1] ₂ PF ₆	2:1	Triclinic	Metal
[(<i>rac</i>)-2]ClO ₄	1:1	Triclinic	Poor semiconductor
[(<i>R</i>)-2]ClO ₄	1:1	Triclinic	Poor semiconductor
[(<i>rac</i>)-2]PF ₆ •(C ₄ H ₈ O)	1:1	Triclinic	Poor semiconductor
[(<i>R</i>)-2] ₂ PF ₆	2:1	Triclinic	Semiconductor
[(<i>S</i>)-2] ₂ PF ₆	2:1	Triclinic	Semiconductor

In the [(*rac*)-1]ClO₄ salt, which should be a poor semiconductor with an indirect gap, the donors are fully oxidized and arrange in centrosymmetric dimers. In sharp contrast, the donors form a β-type packing in the mixed-valence enantiopure salts [(*R*)-1]₂ClO₄ and [(*S*)-1]₂ClO₄ salts, which show metal-like behavior in the high-temperature regime, in agreement with extended Hückel band structure calculations. From a structural, electron transport properties and electronic structure point of view, these enantiopure salts resemble the (1)₂PF₆ and (DM-EDT-TTF)₂XF₆ (X = As, Sb) series, but not to the enantiopure (DM-EDT-TTF)₂ClO₄ compounds [17], pointing out that the variation of the number of stereogenic centers and the use of racemic or enantiopure forms in combination with various anions is a simple mean of reaching a large collection of chiral molecular conductors with original electronic structures. Indeed, both donors 1 and DM-EDT-TTF provided mixed-valence salts of 2:1 stoichiometry with the ClO₄[−] anion, showing metal-like conductivity, yet their crystal structures are drastically different, i.e., monoclinic space group for [(*R*)-1]₂ClO₄ and [(*S*)-1]₂ClO₄ and enantiomorphic hexagonal space groups for [(*R,R*)-DM-EDT-TTF]₂ClO₄ and [(*S,S*)-DM-EDT-TTF]₂ClO₄ [17]. This is a clear consequence of the different number of stereogenic centers and symmetry of the donor, impacting the intermolecular hydrogen bonding interactions with the anion and the overlap interactions between the donors. Further work in these families of materials will be devoted to conductivity measurements under pressure and under a magnetic field, and to the use of larger octahedral or tetrahedral anions.

Supplementary Materials: The following are available online at <http://www.mdpi.com/2073-4352/10/11/1069/s1>, Figure S1: Packing diagram of [(*rac*)-1]ClO₄ in the *ac* plane with an emphasis on the short lateral S⋯S contacts, Figure S2: Solid state structure of [(*rac*)-1]ClO₄ with an emphasis on the C–H⋯O short contacts, Figure S3: Molecular structure of [(*R*)-2]ClO₄ along with the atom numbering scheme, Figure S4: Packing diagram of [(*R*)-2]ClO₄, with an emphasis on the intradimer S⋯S short contacts, Figure S5: Solid state structure of [(*rac*)-2]ClO₄ with an emphasis on the C–H⋯O short contacts, Figure S6: Solid state structure of [(*R*)-2]ClO₄ with an emphasis on the C–H⋯O short contacts, Figure S7: Temperature dependence of the electrical resistivity ρ for a single crystal of [(*rac*)-2]ClO₄ measured using two contacts, Figure S8: Extended Hückel band structure for the donor lattice of [(*rac*)-2]ClO₄, Figure S9: Extended Hückel band structure (a) and Fermi surface (b) for the donor layers of [(*S*)-1]₂ClO₄, Table S1: Selected C=C and C–S bond lengths for [(*rac*)-2]ClO₄ and [(*R*)-2]ClO₄.

Author Contributions: N.A. conceived and designed the experiments; N.M. synthesized and characterized the materials; N.V. performed the chiral HPLC separation of the precursors; P.A.-S., E.B.L. and M.A. investigated the electron transport properties; E.C. undertook the theoretical study; N.A. and E.C. wrote and/or reviewed the manuscript with contributions from all authors. All authors have read and agreed to the published version of the manuscript.

Funding: This research was partially funded in France by the National Agency for Research (ANR), Project 15-CE29-0006-01 ChiraMolCo, in Spain by the Spanish MICIU through Grant PGC2018-096955-B-C44 and the Severo Ochoa FUNFUTURE (CEX2019-000917-S) Excellence Center distinction, as well as by Generalitat de Catalunya (2017SGR1506) and in Portugal by FCT under contracts UIDB/04349/2020 and LISBOA-01-0145-FEDER-029666.

Acknowledgments: This work was supported in France by the CNRS and the University of Angers. The collaboration between the Portuguese and French team members was also supported by a FCT–French Ministry of Foreign Affairs bilateral action FCT/PHC-PESSOA 2020-21 (Project 44647UB).

Conflicts of Interest: The authors declare no conflict of interest.

References

1. Pop, F.; Zigon, N.; Avarvari, N. Main-Group-Based Electro- and Photoactive Chiral Materials. *Chem. Rev.* **2019**, *119*, 8435–8478. [[CrossRef](#)] [[PubMed](#)]
2. Avarvari, N.; Wallis, J.D. Strategies towards Chiral Molecular Conductors. *J. Mater. Chem.* **2009**, *19*, 4061–4076. [[CrossRef](#)]
3. Pop, F.; Avarvari, N. Chiral Metal-Dithiolene Complexes. *Coord. Chem. Rev.* **2017**, *346*, 20–31. [[CrossRef](#)]
4. Mroweh, N.; Auban-Senzier, P.; Vanthuynne, N.; Canadell, E.; Avarvari, N. Chiral EDT-TTF precursors with one stereogenic centre: Substituent size modulation of the conducting properties in the (R-EDT-TTF)₂PF₆ (R = Me or Et) series. *J. Mater. Chem. C* **2019**, *7*, 12664–12673. [[CrossRef](#)]
5. Pop, F.; Auban-Senzier, P.; Frąckowiak, A.; Ptaszyński, K.; Olejniczak, I.; Wallis, J.D.; Canadell, E.; Avarvari, N. Chirality Driven Metallic versus Semiconducting Behavior in a Complete Series of Radical Cation Salts Based on Dimethyl-Ethylenedithio-Tetrathiafulvalene (DM-EDT-TTF). *J. Am. Chem. Soc.* **2013**, *135*, 17176–17186. [[CrossRef](#)]
6. Pop, F.; Auban-Senzier, P.; Canadell, E.; Avarvari, N. Anion size control of the packing in the metallic versus semiconducting chiral radical cation salts (DM-EDT-TTF)₂XF₆ (X = P, As, Sb). *Chem. Commun.* **2016**, *52*, 12438–12441. [[CrossRef](#)]
7. Mroweh, N.; Pop, F.; Mézière, C.; Allain, M.; Auban-Senzier, P.; Vanthuynne, N.; Alemany, P.; Canadell, E.; Avarvari, N. Combining chirality and hydrogen bonding in methylated ethylenedithio-tetrathiafulvalene primary diamide precursors and radical cation salts. *Cryst. Growth Des.* **2020**, *20*, 2516–2526. [[CrossRef](#)]
8. Wallis, J.D.; Karrer, A.; Dunitz, J.D. Chiral metals? A chiral substrate for organic conductors and superconductors. *Helv. Chim. Acta* **1986**, *69*, 69–70. [[CrossRef](#)]
9. Mroweh, N.; Mézière, C.; Allain, M.; Auban-Senzier, P.; Canadell, E.; Avarvari, N. Conservation of structural arrangements and 3:1 stoichiometry in a series of crystalline conductors of TMTTF, TMTSF, BEDT-TTF, and chiral DM-EDT-TTF with the oxo-bis[pentafluorotantalate(V)] dianion. *Chem. Sci.* **2020**, *11*, 10078–10091. [[CrossRef](#)]
10. Matsumiya, S.; Izuoka, A.; Sugawara, T.; Taruishi, T.; Kawada, Y. Effect of Methyl Substitution on Conformation and Molecular Arrangement of BEDT-TTF Derivatives in the Crystalline Environment. *Bull. Chem. Soc. Jpn.* **1993**, *66*, 513–522. [[CrossRef](#)]
11. Matsumiya, S.; Izuoka, A.; Sugawara, T.; Taruishi, T.; Kawada, Y.; Tokumoto, M. Crystal Structure and Conductivity of Chiral Radical Ion Salts (Me₂ET)₂X. *Bull. Chem. Soc. Jpn.* **1993**, *66*, 1949–1954. [[CrossRef](#)]
12. Pop, F.; Allain, M.; Auban-Senzier, P.; Martínez-Lillo, J.; Lloret, F.; Julve, M.; Canadell, E.; Avarvari, N. Enantiopure Conducting Salts of Dimethylbis(ethylenedithio)tetrathiafulvalene (DM-BEDTTTF) with the Hexachlororhenate(IV) Anion. *Eur. J. Inorg. Chem.* **2014**, *2014*, 3855–3862. [[CrossRef](#)]
13. Karrer, A.; Wallis, J.D.; Dunitz, J.D.; Hilti, B.; Mayer, C.W.; Bürkle, M.; Pfeiffer, J. Structures and Electrical Properties of Some New Organic Conductors Derived from the Donor Molecule TMET (S,S,S,S-Bis(dimethylethylenedithio) tetrathiafulvalene). *Helv. Chim. Acta* **1987**, *70*, 942–953. [[CrossRef](#)]
14. Pop, F.; Laroussi, S.; Cauchy, T.; Gómez-García, C.J.; Wallis, J.D.; Avarvari, N. Tetramethyl-Bis(ethylenedithio)-Tetrathiafulvalene (TM-BEDT-TTF) Revisited: Crystal Structures, Chiroptical Properties, Theoretical Calculations, and a Complete Series of Conducting Radical Cation Salts. *Chirality* **2013**, *25*, 466–474. [[CrossRef](#)] [[PubMed](#)]
15. Yang, S.; Pop, F.; Melan, C.; Brooks, A.C.; Martin, L.; Horton, P.; Auban-Senzier, P.; Rikken, G.L.J.A.; Avarvari, N.; Wallis, J.D. Charge transfer complexes and radical cation salts of chiral methylated organosulfur donors. *CrystEngComm* **2014**, *16*, 3906–3916. [[CrossRef](#)]
16. Pop, F.; Batail, P.; Avarvari, N. Enantiopure Radical Cation Salt Based on Tetramethyl-bis(ethylenedithio)-tetrathiafulvalene and Hexanuclear Rhenium Cluster. *Crystals* **2016**, *6*, 8. [[CrossRef](#)]
17. Pop, F.; Auban-Senzier, P.; Canadell, E.; Rikken, G.L.J.A.; Avarvari, N. Electrical magneto-chiral anisotropy in a bulk chiral molecular conductor. *Nat. Commun.* **2014**, *5*, 3757. [[CrossRef](#)]
18. Kini, A.M.; Parakka, J.P.; Geiser, U.; Wang, H.-H.; Rivas, F.; DiNino, E.; Thomas, S.; Dudek, J.D.; Williams, J.M. Tetraalkyl- and dialkyl-substituted BEDT-TTF derivatives and their cation-radical salts: Synthesis, structure, and properties. *J. Mater. Chem.* **1999**, *9*, 883–892. [[CrossRef](#)]

19. Zambounis, J.S.; Mayer, C.W.; Hauenstein, K.; Hilti, B.; Hofherr, W.; Pfeiffer, J.; Bürkle, M.; Rihs, G. Crystal Structure and Electrical Properties of κ -((S,S)-DMBEDT-TTF)₂ClO₄. *Adv. Mater.* **1992**, *4*, 33–35. [[CrossRef](#)]
20. Mroweh, N.; Mézière, C.; Pop, F.; Auban-Senzier, P.; Alemany, P.; Canadell, E.; Avarvari, N. In Search of Chiral Molecular Superconductors: κ -((S,S)-DM-BEDT-TTF)₂ClO₄ Revisited. *Adv. Mater.* **2020**, *32*, 2002811. [[CrossRef](#)]
21. Chaikin, P.M.; Kwak, J.F. Apparatus for thermopower measurements on organic conductors. *Rev. Sci. Instrum.* **1975**, *46*, 218–220. [[CrossRef](#)]
22. Almeida, M.; Alcácer, L.; Oostra, S. Anisotropy of thermopower in N-methyl-N-ethylmorpholinium bistetracyanoquinodimethane, MEM(TCNQ)₂, in the region of the high-temperature phase transitions. *Phys. Rev. B* **1984**, *30*, 2839–2844. [[CrossRef](#)]
23. Lopes, E.B. *INETI-Sacavém*; Internal Report; INETI Press: Sacavém, Portugal, 1991.
24. Huebener, R.P. Thermoelectric Power of Lattice Vacancies in Gold. *Phys. Rev.* **1964**, *135*, A1281–A1291. [[CrossRef](#)]
25. Whangbo, M.-H.; Hoffmann, R. The Band Structure of the Tetracyanoplatinate Chain. *J. Am. Chem. Soc.* **1978**, *100*, 6093–6098. [[CrossRef](#)]
26. Ammeter, J.H.; Bürgi, H.-B.; Thibault, J.; Hoffmann, R. Counterintuitive Orbital Mixing in Semiempirical and ab Initio Molecular Orbital Calculations. *J. Am. Chem. Soc.* **1978**, *100*, 3686–3692. [[CrossRef](#)]
27. Pénicaud, A.; Boubekeur, K.; Batail, P.; Canadell, E.; Auban-Senzier, P.; Jérôme, D. Hydrogen-Bond Tuning of Macroscopic Transport Properties from the Neutral Molecular Component Site along the Series of Metallic Organic-Inorganic Solvates (BEDT-TTF)₄Re₆Se₅C₁₉·[guest], [guest = DMF, THF, dioxane]. *J. Am. Chem. Soc.* **1993**, *115*, 4101–4112. [[CrossRef](#)]
28. Mori, T. Structural Genealogy of BEDT-TTF-Based Organic Conductors I. Parallel Molecules: β and β'' Phases. *Bull. Chem. Soc. Jpn.* **1998**, *71*, 2509–2526. [[CrossRef](#)]
29. Whangbo, M.-H.; Williams, J.M.; Leung, P.C.W.; Beno, M.A.; Emge, T.J.; Wang, H.H. Role of the Intermolecular Interactions in the Two-Dimensional Ambient-Pressure Organic Superconductors β -(ET)₂I₃ and β -(ET)₂IBr₂. *Inorg. Chem.* **1985**, *24*, 3500–3502. [[CrossRef](#)]

Publisher's Note: MDPI stays neutral with regard to jurisdictional claims in published maps and institutional affiliations.



© 2020 by the authors. Licensee MDPI, Basel, Switzerland. This article is an open access article distributed under the terms and conditions of the Creative Commons Attribution (CC BY) license (<http://creativecommons.org/licenses/by/4.0/>).